

# Systematic Method for Positioning Clamps and Strongbacks Based on their Influence on Welding Displacements

Donghan Woo, Mitsuru Kitamura\*, Akihiro Takezawa  
Dept. of Transportation and Environmental Systems, Hiroshima University  
Higashi-Hiroshima City, Japan

## Abstract

To control welding displacements, mitigation methods such as clamps and strongbacks are widely used in heavy industries. It can be easily concluded that providing for as many clamps and strongbacks as feasible on welded structures to minimize welding displacements is common knowledge, but this may not always be feasible due to restrictive work environments as well as cost factors and interference from other portions of the structure. Currently there is not a distinct system to efficiently position clamps and strongbacks at welded structures. Based on understanding of how clamps and strongbacks effect on the reduction of welding displacements, a systematic method to efficiently position them will enable improvements to the welding process. In the present study, several cases which have differently positioned clamps and strongbacks at welded structures were numerically simulated by the elastic Finite Element Method (FEM) using inherent strain theory to investigate the influence of clamps and strongbacks on the reduction of welding distortions. According to the simulation data, the applicable systematic method for efficiently positioning clamps and strongbacks for minimizing welding deformations is proposed herein.

KEY WORDS: Welding sequence; welding displacement; ship grillage structure; Inherent strain; FEM

## Nomenclature

<i>Abbreviation</i>	
FEM	Finite element method
MPC	Multipoint constraint function
HT	High strength steel
<i>Symbols</i>	
$A_{displacement} = \frac{\sum_{k=1}^n  z_k }{n}$	Average of the absolute values of the z-axis displacement of all the bottom plate nodes (mm)
$b$	Width of the element along the welding line [mm]
$c$	Specific heat [J/kg/K]
$C_t(L)$	Welding length compensation coefficient for lateral shrinkage
$C_a(L)$	Welding length compensation coefficient for angular deformation
$E$	Young's modulus [MPa]
$F_T$	Contraction force [N]
$h$	Plate thickness [mm]
$L$	Welding length [mm]
$n$	Total number of nodes of a bottom plate
$Q^*$	Heat input [J/mm <sup>3</sup> ]
$Q_{net}$	Net heat input [J/mm]
$S$	Transverse shrinkage [mm]
$S_0$	Transverse shrinkage at a welding length of 200 mm [mm]

$\nu$	Poisson's ratio
$z_k$	Z-axis displacement of a node of a bottom plate [mm]
$\alpha$	Linear expansion coefficient [1/K]
$\sigma_Y$	Yield stress [MPa]
$\rho$	Density [kg/m <sup>3</sup> ]
$\theta$	Angular deformation
$\theta_0$	Angular deformation at a welding length of 200 mm
$\varepsilon^{total}$	Total strain
$\varepsilon^{elastic}$	Elastic strain
$\varepsilon^{thermal}$	Thermal strain
$\varepsilon^{plastic}$	Plastic strain
$\varepsilon^{creep}$	Creep strain
$\varepsilon^{phase}$	Phase transformation
$\varepsilon^* = \varepsilon^{inherent}$	Inherent strain
$\varepsilon_l^*$	Inherent strain of longitudinal shrinkage
$\varepsilon_t^*$	Inherent strain of transverse shrinkage
$\varepsilon_a^*$	Inherent strain of angular distortion

## 1. Introduction

In the welding process, welding distortions are unavoidably caused by local shrinkages and angular distortions along welding lines under thermal cycles. Precisely predicting welding displacements of complex structures with multiple stiffeners is highly difficult. These unexpected displacements result in misalignment between separately welded structures during final assembling work and reduce structural safety. To mitigate welding distortion, there have been many fundamental studies. Substituting the arc welding with laser or electron beam to minimize heat input was proposed (Michaleris, 2011). The optimal groove type of weld and its sequence for the reduction of welding distortion was investigated (Ye et al., 2015). The welding sequence is an essential factor for mitigating welding distortions of welded structures (Chen et al., 2015). Despite these approach, fundamental method in practical engineering, external constraints such as clamping and strongbacks are mainly used to control welding distortion. Prior to the start of the welding process, welded structures are usually clamped on the side to constrain their movement. Strongbacks are temporarily attached to welded structures to improve not only the stiffness of structures, but also reduce local displacements during welding process. But this leads to high production costs; and wrongly positioned clamps and strongbacks could lead to unexpected welding displacements.

There have been many studies to investigate the effect of external constraints on welding distortions. Liu and Zhang (2009) investigated the influence of external load on the improvement of the reduction of angular distortion caused by welding. Schenk et al. (2009) demonstrated that different clamping conditions strongly affected the residual stresses and welding displacement. The effect of welding fixtures used in robotic cells on car bodies based on the modular concept was validated using a methodological approach (Hajduk et al., 2011). Park et al. (2012) investigated the effects of external loads on welding displacement, angular distortion, and residual stresses caused by different levels of pre-tension stress. Ma et al. (2015; 2017) studied the jig constraint effect on welding distortions of large structures using experimental and computational methods. Although many studies have thoughtfully validated the role of external constraints for the mitigation of welding deformations, they did not discuss about an applicable guideline for efficiently positioning external constraints.

Due to the limitation of the experimental method to predict welding distortions of large and complex structures, computation methods were introduced. To predict the effect of the change in temperature along welding lines and determine the welding displacement, thermal elastic-plastic FEM has been typically used by researchers in various studies. The major drawback of this method is that they require lengthy calculation times, especially when analyzing complex and large structures. To tackle this problem, Luo et al. (1997) introduced the concept of inherent strain as the initial strain along welding lines in the elastic FEM, to be able to consider the effect of the change in temperature. Liang et al. (2005) proposed a simple and efficient method to estimate inherent deformation using thermal elastic-plastic FEM and experiments. The inherent strain has been found to be capable of precisely predicting the welding distortion of a large plate structures. Deng et al. (2007) have validated the inherent strain theory by the results obtained using this theory with experiment results on welded plane structures. Wang et al. (2011) demonstrated that inherent strain method is capable of calculating angular welding displacement with reasonable accuracy. To obtain the accurate results from the numerical simulation of complex and large structures, the relationship between the different sequentially welded structures is important, and therefore, an interface element as an efficient method to handle this relationship was introduced (Deng et al., 2004).

As above discussed studies, the application of inherent strain theory in the elastic FEM for precisely predicting welding distortion was

obviously validated with comparing numerical calculation database and experimental measurement results. Furthermore, the effect of different welding sequences and external constraints on welding deformation was validated with using inherent strain method and experiment database. However, there was not an applicable guideline which efficiently positioning clamps and strongbacks for minimizing welding distortions. Thus, they are injudiciously positioned as many as possible. In the present study, several numerical simulations using the inherent strain in the elastic FEM are used to investigate the influence of clamps and strongbacks on the reduction of welding distortions of large and complex structures. According to those computation data, systematic methods for efficiently positioning clamps and strongbacks are investigated.

## 2. Theory of Numerical Simulation for Welding

To reduce significant calculation time and be able to realize the sequence-based analysis, in-house developed code which based on the elastic FEM with the application of inherent strains is employed. Additionally, MPC and interface element are assigned along welding line to consider the effect of gap and misalignment in the welding sequence. In-house developed code has iteration logic system as Fig. 1.

### 2.1 Inherent Strain Approach

Based on thermal elastic-plastic FEM and experimental observation, Ueda et al. (1993) pointed out that the inherent strain  $\epsilon^{inherent}$  causes welding distortions and residual stress along welding line. During the heating and cooling cycle of welding process, the component of the total strain  $\epsilon^{total}$  is given as Eq. (1). When the welding heat finally disappears, the inherent strain is the sum of inelastic strain components as Eq. (2). In particular, the plastic strain  $\epsilon^{plastic}$  is the representative of the inherent strain because the creep strain  $\epsilon^{creep}$  and the phase transformation  $\epsilon^{phase}$  are negligibly small (Murakawa et al., 2012). As Fig. 2, the inherent strain produces welding deformations which are clarified into transverse shrinkage  $S$ , angular distortion  $\theta$  and longitudinal shrinkage which results in a contraction force  $F_T$  that can be used in elastic simulation to improve results. The inherent strain could be considered as existing in a limited portion near the welding line, thus inherent strain is constantly applied to limited elements which are positioned along welding lines (Murakawa et al., 2012).

$$\epsilon^{total} = \epsilon^{elastic} + \epsilon^{thermal} + \epsilon^{plastic} + \epsilon^{creep} + \epsilon^{phase} \quad (1)$$

$$\begin{aligned} \epsilon^* &= \epsilon^{inherent} \\ &= \epsilon^{total} - \epsilon^{elastic} \\ &= \epsilon^{thermal} + \epsilon^{plastic} + \epsilon^{creep} + \epsilon^{phase} \end{aligned} \quad (2)$$

#### 2.1.1 Calculation of Inherent Deformation

An initial measurement of the welding deformation on a simple plane structure is necessary to predict the magnitude of the local shrinkages. For a particular welding condition, the measurement process is performed both experimentally and by using a thermal elastic-plastic finite element model. Based on the measured welding displacement, the equations for the inherent deformation can be derived, so that the obtained displacements from the numerical model match the experimental results. Based on the experimental data, Japan Shipbuilding Research Association (2000) derived Eqs. (3) ~ (5) to be able to calculate arc butt welding's inherent deformations of HT50 steel plate which is widely used to build ships and offshore structures. The experiment measured the welding deformation caused by 200mm length welding at the middle of the square HT50 steel plain plate (200 mm × 200 mm × 10 mm). Table 1 shows the mechanical property HT50 steel.

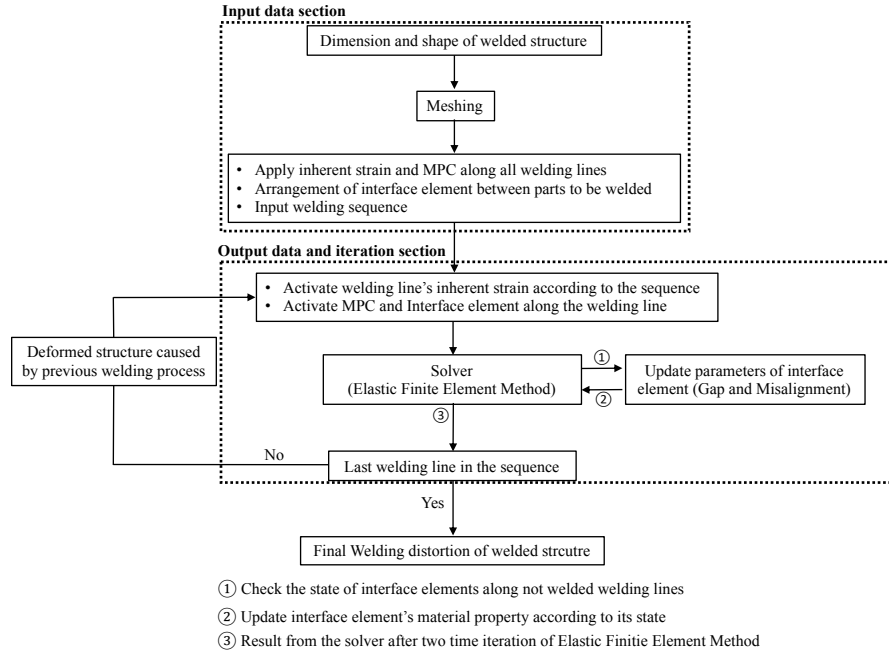


Fig. 1. Analysis procedure logic by the sequence of elastic FEM

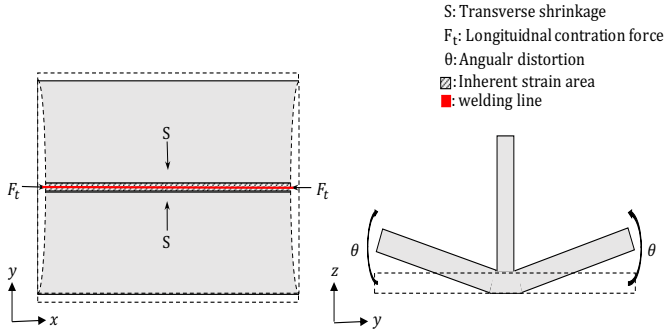


Fig. 2. Application of inherent strain along welding line

In these equations, the amount of the inherent deformations are decided by the amount of the heat input  $Q^*$  of the arc butt welding. Kuniyiko et al. (1976) validated that the relationship between the heat input  $Q^*$  and the net heat input  $Q_{net}$  in the welding process is decided by the amount of the thickness  $h$  of the welded steel plate and can be expressed as  $Q^* = Q_{net}/h^2$ . White et al. (1980) concluded that the longitudinal shrinkage is generally evaluated by the contraction force  $F_T$ ; the relationship between the contraction force  $F_T$  and the net heat input  $Q_{net}$  is derived as Eq. (5).

Table 1. Mechanical property of HT50 steel

Density [kg/m <sup>3</sup> ]	Young's Modulus [MPa]	Specific heat [J/kg/°C]	Yield stress [MPa]	Poisson's ratio
7720	$2.0 \times 10^5$	659.4	440	0.3

#### 1) Transverse shrinkage

$$S = C_t(L)S_0 \quad (3)$$

$$S_0 = \begin{cases} 1.16 \times 10^{-3} Q_{net}/h & (Q^* \leq 6.27) \\ h\{1.44 \times 10^{-4}[(Q^*)^2 - Q^*] + 2.5 \times 10^{-3}\} & (6.27 < Q^* \leq 20) \\ 2.85 \times 10^{-3} Q_{net}/h & (20 < Q^*) \end{cases}$$

$$C_t(L) = [4 \tan^{-1}(L/200) + (L/100) \times \log(1 + 40000/L^2)]/3.74$$

#### 2) Angular deformation

$$\theta = C_a(L)\theta_0 \quad (4)$$

$$\theta_0 = \begin{cases} 1.44 \times 10^{-3} Q^* & (Q^* \leq 6.27) \\ 1.06 \times 10^{-1} Q^* / \{(Q^* - 6.16)^2 + 73.6\} & (6.27 < Q^*) \end{cases}$$

$$C_a(L) = [8 \tan^{-1}(L/120) + (1 + \nu)(L/60) \times \log(1 + 14400/L^2)]/8.84$$

#### 3) Longitudinal shrinkage (contraction force)

$$F_T = 0.2Q_{net} \quad (5)$$

#### 2.1.2 Calculation of Inherent Strain

The inherent strain causing transverse and longitudinal shrinkage remains uniformly distributed toward the surface and out-of-plane deformation, and the bending strain causing angular distortion is linearly distributed against the direction of thickness (Ueda et al., 1993). The width of the element that produced the equivalent inherent strain is decided by the condition of the welding process. It is desirable to establish the correlation here. If the maximum temperature is  $T = \sigma_Y/E\alpha$  ( $\alpha$ : linear expansion coefficient) and the heat source is approximated to the instantaneous line heat source, the width  $b$  is defined as Eq. (6), (Kuniyiko et al., 1976).

$$b = \sqrt{0.117(\alpha/c\rho)(E/\sigma_Y)Q_{net}} \quad (6)$$

When the element width is  $b$ , inherent strain of longitudinal shrinkage, transverse shrinkage and angular distortion can be defined as Eqs. (7) ~ (9) (Japan Shipbuilding Research Association, 2000). Angular deformation is defined as the bending stress to elements that the inherent strain is applied. The progress of the angular deformation changes the inherent strain.  $k = \theta/b$  is the curvature of the deformation.

$$\varepsilon_l^* = 0.5(F_T/(Ehb)) \quad (7)$$

$$\varepsilon_t^* = 0.5(S/b) \quad (8)$$

$$\varepsilon_a^* = -hk \quad (9)$$

## 2.2 Interface element function

In the welding simulations of the complex structures, local shrinkages, gaps, and misalignments commonly occur in the two components being welded, and they have a significant effect on the final welding displacements. Therefore, it is important to define the relationship between the fully welded parts and the newly welded parts to consider the effect of gaps and misalignments caused by local shrinkage while welding process in the numerical simulations. Interface elements have been incorporated into the model to represent the space between the two parts and to model misalignments and gaps. These elements use a nonlinear spring model. Prior to the welding operation along the weld line, the stress in the interface elements is measured to determine if the stress is inducing tension or compression in the interface elements. If it is determined that the stress is inducing tension, then the interface elements are represented in the model as freely stretched. On the other hand, if the stress is compressive in nature, the interface elements are modeled as fully compressed, such that the two parts are touching each other. Fig. 3 shows these two alternate possible states of the interface elements. Interface elements are positioned along all welding lines in the simulation.

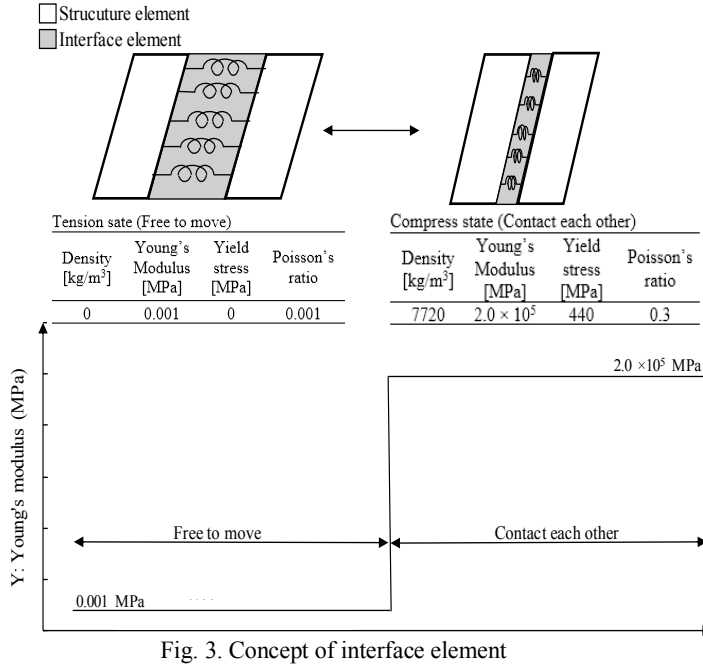


Fig. 3. Concept of interface element

## 2.3 Multipoint Constraint Function

Multipoint constraint function (MPC) is used to model fully welded parts in the FEM analysis. Fig. 4 depicts the use of MPCs to model the weld joint between node 1 and node 2. The displacements of the two nodes, which were initially separated, have the same values after activating MPC. In other words, using MPC allows the two nodes to move together during the welding sequence. The tack weld, whose function is to temporarily attach the two parts being welded, is used in this simulation of MPC. In Fig. 4, nodes a and b are tack-welded. These nodes are initially represented using MPC. Nodes c, d, e, f, g, and h each move freely prior to using MPC. This free movement leads to gaps and misalignments in the structure.

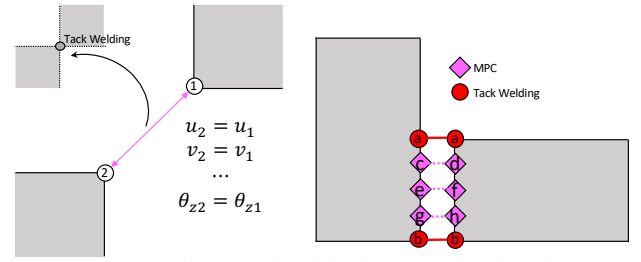


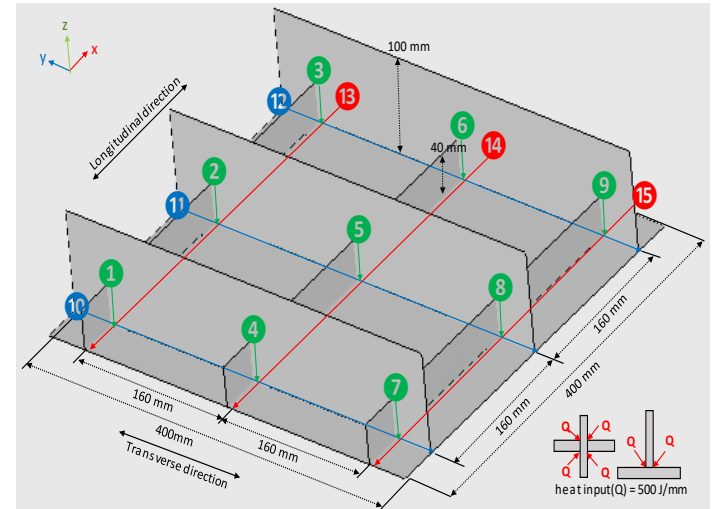
Fig. 4. Application of multipoint constraint function

## 3. Analysis of Model Dimensions and Boundary Conditions

A simple square-shaped grillage structure of 400 mm × 400 mm is employed as shown in Fig. 5. Larger and smaller stiffeners are placed in transverse and longitudinal directions, respectively, to analyze the effects of the positions of clamps and strongbacks for preventing the structures from welding deformation. The length, height and thickness of stiffeners are also listed in Fig. 5. Additionally, a general ship grillage structure is employed as Fig. 6 for clearly validating the effects of these positions to welding deformation. The ship grillage structure of 3000 mm × 2000 mm is relatively large and has the different composition of stiffeners. The length, height and thickness of stiffeners are listed in Fig. 6. The welding sequence of all weld lines is schematically drawn by circled numbers in Fig. 5 and Fig. 6. The vertical welds are finished first, and the transverse welds and longitudinal welds are sequentially performed (Woo et al., 2019). Table 2 shows the arc butt welding condition. The cross points at both ends of welding lines are tack-welded prior to the full welding of the structure.

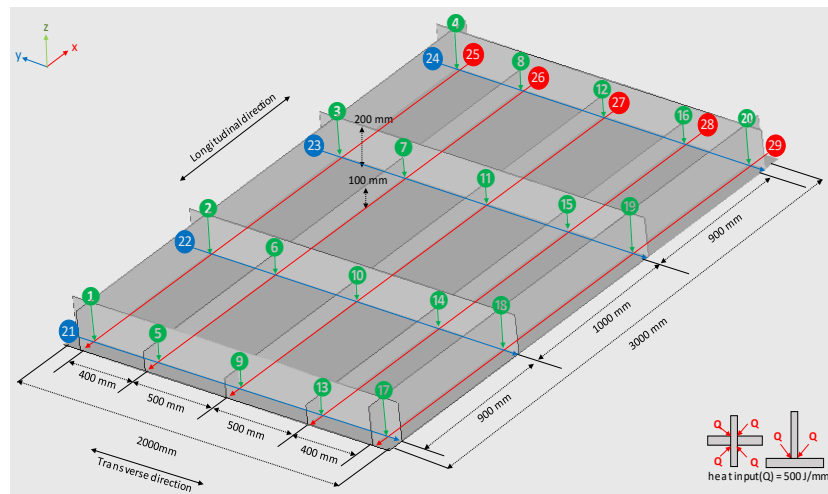
Table 2. Arc butt welding Conditions

Current [A]	Voltage [V]	Travel speed [mm/s]	Heat efficiency	Net heat [J/mm²]
230	23	5	0.77	500



Part	Dimension (mm)
Bottom plate	400 × 400 × 10
Longitudinal stiffener (x-axis)	400 × 40 × 10
Transverse stiffener (y-axis)	400 × 100 × 10

Fig. 5. Square Shape Grillage Structure (400 mm × 400 mm)



Part	Dimension (mm)
Bottom plate	3000 × 2000 × 10
Longitudinal stiffener (x-axis)	3000 × 200 × 10 3000 × 100 × 10
Transverse stiffener (y-axis)	2000 × 200 × 10

Fig. 6. General Ship Grillage Structure (3000 mm × 2000 mm)

Case A-1. Basic 4 clamps

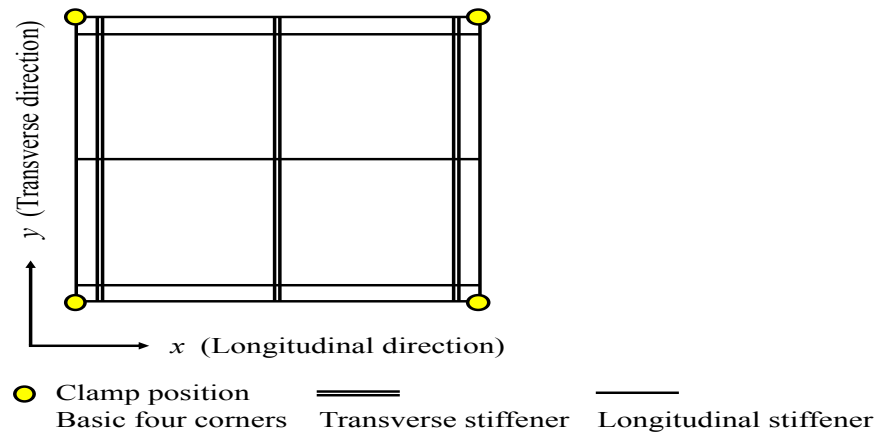


Fig. 7. Z-axis displacement of the bottom plate of Case A-1

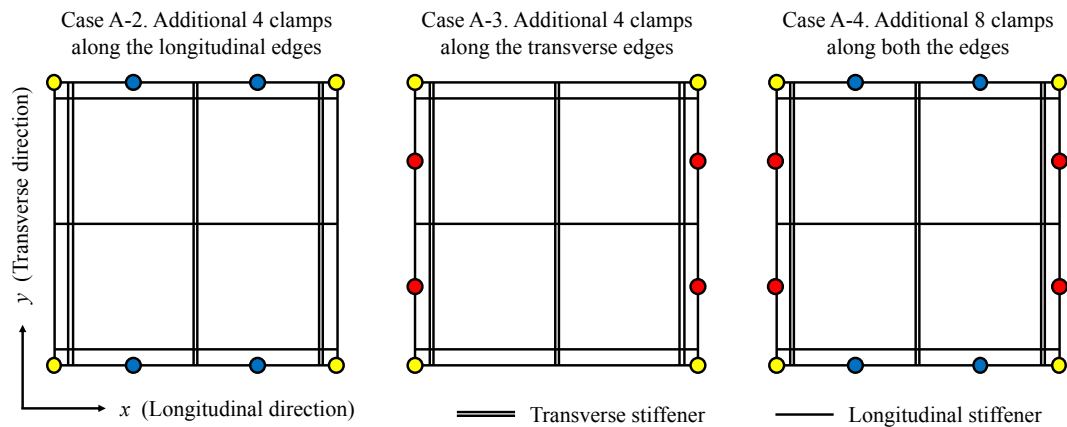


Fig. 8. Additional clamping cases (Square shape grillage structure 400 mm × 400 mm)

#### 4. Effect of Additional Clamps and Efficient Positioning of Clamps to reduce Welding Displacements of the Square-Shaped Grillage Structure

During welding process, clamps are widely used to hold the structures in place. Basically, Clamps are positioned at the points where larger displacements are expected along the edge of welded structures for improving their performances. In the numerical simulation, clamps are defined by completely fixing the nodes in all axial directions. First, the basic clamping condition that clamps four corners of the bottom plate are applied to the structure. This simulation is noted as Case A-1, and shown in Fig. 7 where yellow circles indicate the basic clamps. Additional clamps are basically positioned at nodes which have the highest displacement along each edge of Case A-1. To study the effects of the relationship between the stiffener size and the additional clamp position on the welding displacements, three cases are simulated. These cases are indicated as Cases A-2, A-3 and A-4 as shown in Fig. 8.

A-1: Basic clamps at the corners of bottom plate marked by yellow circles

A-2: Additional clamps along the longitudinal edges marked by blue circles

A-3: Additional clamps along the transverse edges marked by red circles

A-4: Additional clamps along both of the longitudinal and transverse edges

#### 4.1 Results and Discussion of the Effect of Clamping on the Square-Shaped Grillage Structure

Eq. (10) calculating the average absolute value of the z-axis nodal displacement of the bottom plate is used to see the overall effect of the additional clamps. The z-direction displacement distributions of the bottom plate along the selected two lines, ST (Transverse) and SL (Longitudinal), are compared to analyze the effects of clamp positions precisely. These lines are indicated by red lines in Fig. 9. Additionally, the displacement along the lines of TS (Transverse stiffener) and LS (Longitudinal stiffener) of the square-shaped grillage structure are measured to analyze the effect of differently positioned clamps on stiffeners. They are shown by blue lines in Fig. 9.

$$A_{displacement} = \frac{\sum_{k=1}^n |z_k|}{n} \quad (10)$$

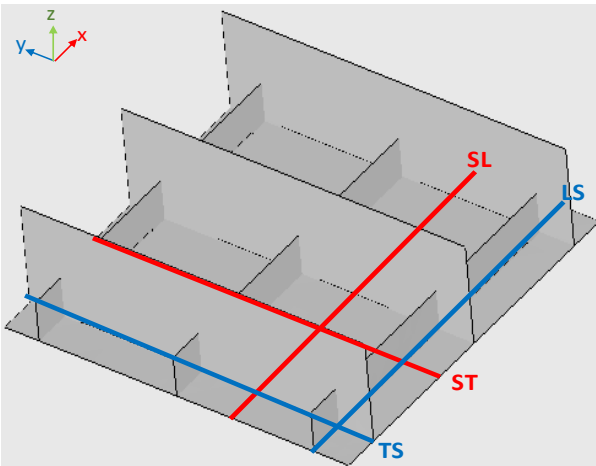


Fig. 9. Measuring line for the displacement distribution of the square-shaped grillage structure

Fig. 10 and 11 show the results of four cases A-1 ~ A-4 using different clamping schemes to hold the side edges of the square-shaped grillage structure. It is observed in Fig. 10 that adding more clamps (Cases A-2, A-3 and A-4) results in 42.7 ~ 55.1% reduction in  $A_{displacement}$  compared to Case A-1. Fig. 11 shows the z-axis displacement distributions of the bottom plate under these clamping schemes. It is noted that severe buckled features appear at the centers of the stiffened plates in Case A-1. Adding more clamps to the side edges of the bottom plate helped to reduce the large displacements along edges and the buckled features. It should be emphasized that  $A_{displacement}$  and the z-axis displacement of the bottom plate of Case A-2 are smaller than those of Case A-3, even though the same total number of clamps have been used in both cases. Case A-4 gives the smallest  $A_{displacement}$  as expected since all edges are clamped.

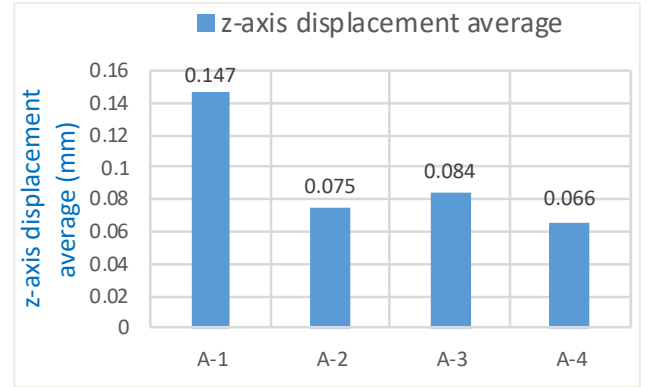


Fig. 10.  $A_{displacement}$  of Cases A-1, A-2, A-3 and A-4

The z-axis displacement distributions along ST and SL are plotted in Fig. 12 and 13, respectively. These figures clearly show the difference in the efficacies of clamps between Cases A-2 and A-3. The distances of the reduction of Cases A-2, A-3 and A-4 from Case A-1 on line ST are 0.1515 mm, 0.0773 mm and 0.1574 mm which are measured at the highest point of the buckling curve of Case A-1 as shown in Fig. 12. Comparing to Case A-4 which produces the maximum reduction in the z-axis displacement, the efficiencies of Cases A-2 and A-3 for reducing the buckling curve is discussed. In Case A-2, the effect of the additional clamps at longitudinal edges on the reduction of the buckling feature along line ST (96.3%) is higher than SL (83.1%). On the other hand, the additional clamps at transverse edges work more effectively along line SL (67.8%) than ST (49.1%) in Case A-3. Comparing the z-axis displacement distributions along ST and SL for Case A-2, significant differences are observed not only in the displacement value but also in the angle of the displacement curve at the ends of these lines. The displacement curve starts from 0 mm with small slope along ST in Fig. 12 since additional clamp is given at this end point, while a relatively large displacement and slope are seen at the end of SL in Fig. 13. Fig. 14 shows the relationships between the displacements measured lines and clamp positions. Since the additional clamps of Case A-2 are located at both ends of line ST (A2-ST), they are effective to mitigate the buckling feature deformation along this line resulting in the large reduction efficiency of 96.3%. On the other hand, this clamp condition for SL (A2-SL) can't mitigate the buckling feature deformation along line SL directly, so the efficiency of reducing displacement downed to 83.1%. The same kind of relationship is seen in Case A-3 such that the additional clamps at transverse edges worked more effectively along line SL (A3-SL) than ST (A3-ST) since these clamps are located at both ends of line SL. So, it is noted that additional clamps show their high performance in the direction perpendicular to the edge which they are applied.



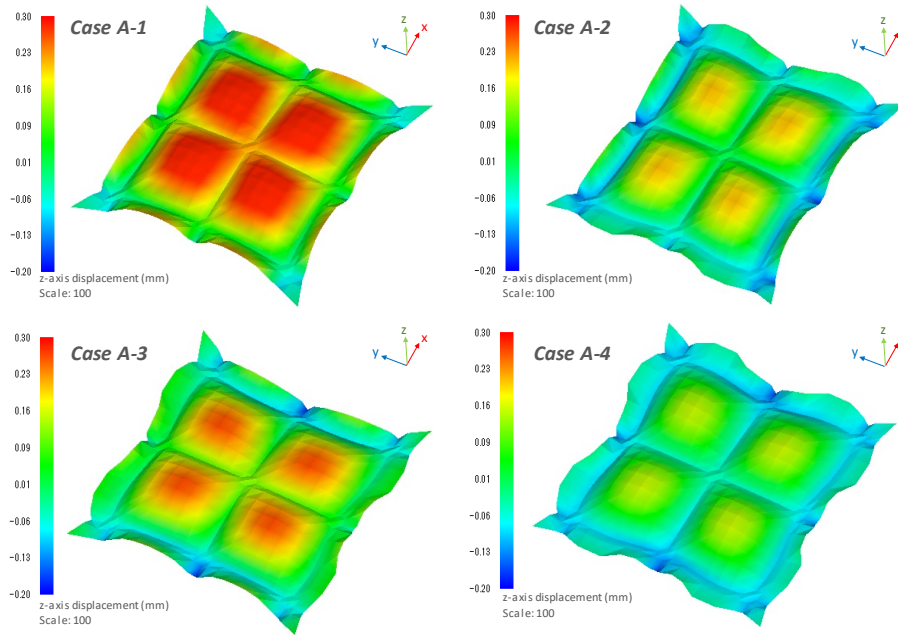


Fig. 11. Z-axis displacement of the bottom plate of Case A-1, A-2, A-3 and A-4

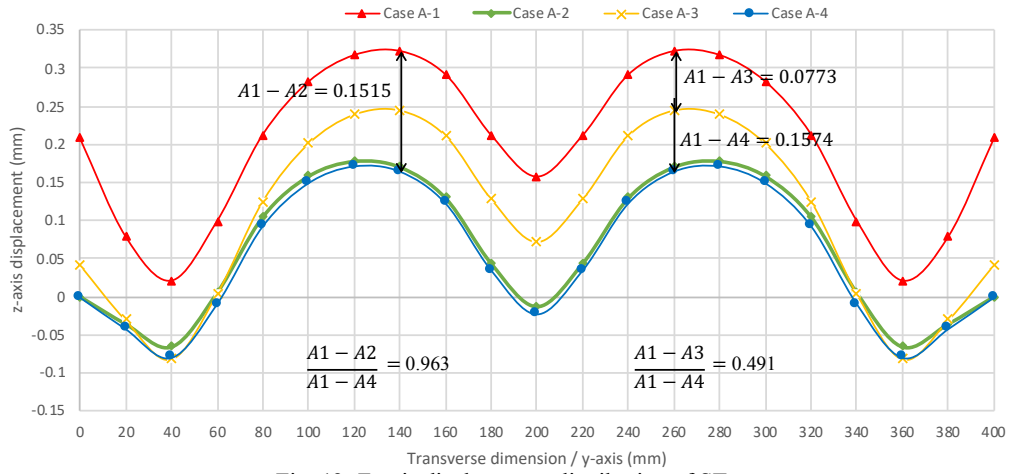


Fig. 12. Z-axis displacement distribution of ST

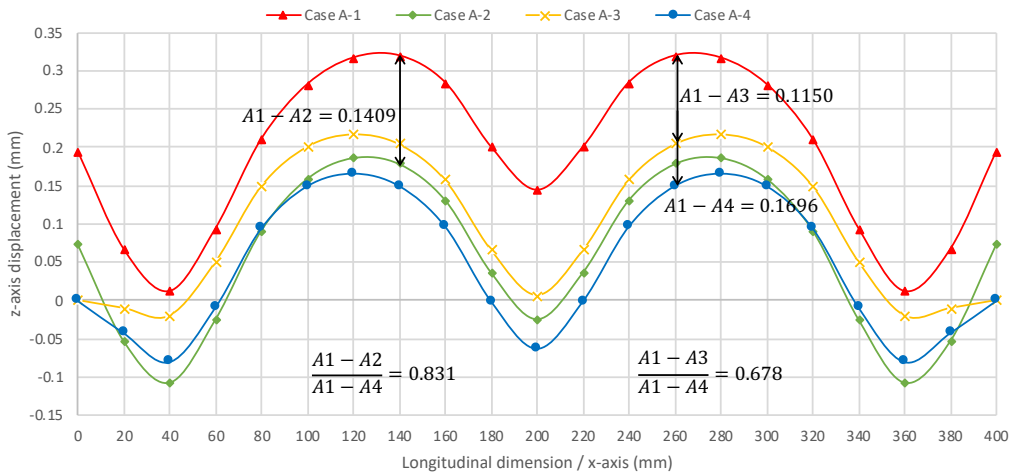


Fig. 13. Z-axis displacement distribution of SL

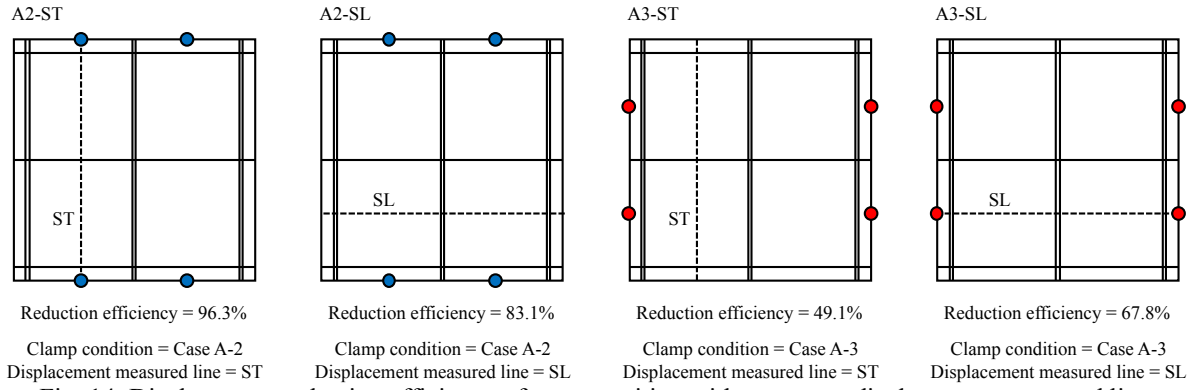


Fig. 14. Displacement reduction efficiency of comp position with respect to displacement measured line

Though the relationship between clamp position and stiffener direction of ST in Case A-2 and that of SL in Case A-3 are the same, the displacement reduction efficiencies are different such as 96.3% and 67.8% (A2-ST and A3-SL in Fig. 14). The structural difference in the longitudinal and transverse directions is only stiffener size. But, the size difference itself doesn't make so large difference in the z-axis displacements along ST and SL since the displacements on these lines for Case A-1 are almost the same as shown in Fig. 12 and 13. This fact indicates the importance of the combination of the stiffener size and the clamp position.

In order to analyze the effects of the additional clamps with respect to the stiffener size, the z-axis displacement distributions on the lines where stiffeners are located are plotted in Fig. 15 and 16. TS and LS indicate the lines of transverse and longitudinal stiffeners, respectively. Although there is little difference between the displacement distributions on TS and LS for Case A-1 having basic 4 clamps, there exist significant differences for Cases A-2 and A-3 having additional

clamps in different sides. In Case A-2, additional clamps on the longitudinal edges directly let the transverse stiffeners as close to a straight line (A2-TS in Fig. 15). Since the longitudinal stiffeners are weaker than the transverse stiffeners, the longitudinal stiffeners follow the deformation created by the transverse stiffeners resulting in its relatively flat deformation (A2-LS in Fig. 16). In Case A-3, additional clamps on the transverse edges make the longitudinal stiffeners relatively flat (A3-LS). But, the longitudinal stiffeners aren't strong enough to prevent the transverse stiffeners from deforming resulting in the large displacement of TS (A3-TS). This is the reason why Case A-2 decreases the welding deformation more than Case A-2, and hence, it is recommended that the additional clamps are placed along the plate edges perpendicular to the larger stiffener direction.

According to the above results and discussions, the systematic method for optimally clamping under limited work environment condition to maximize their efficacy for minimizing welding displacements is proposed as Fig. 17.

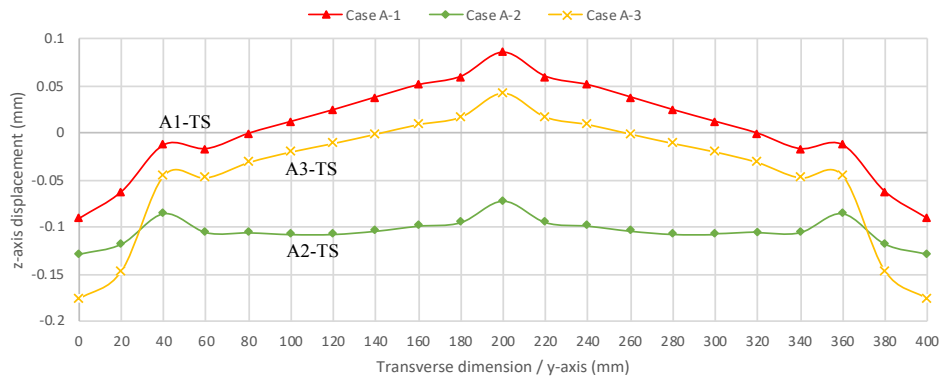


Fig. 15. Z-axis displacement distribution of TS

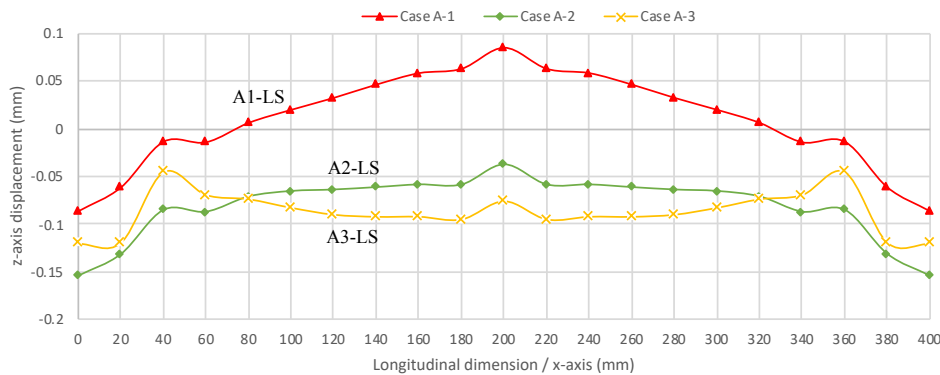


Fig. 16. Z-axis displacement distribution of LS



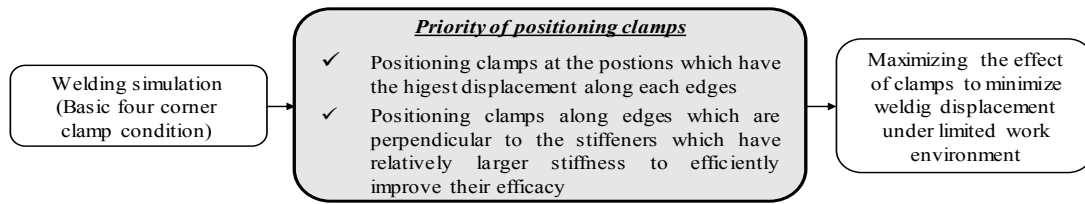


Fig. 17. Systematic method to optimally position clamps under limited work environment

## 5. The Effect of Strongbacks and Efficient Positioning of Strongbacks to Minimize Welding Displacements of the Square-Shaped Grillage Structure

To minimize the welding displacements, strongbacks are temporarily installed on a structure as stiffeners during fabrication. The positioning of these strongbacks is critical, and different results can be obtained depending on their placement on the structure. Therefore, a method to optimally position strongbacks that minimizes welding displacements is essential, especially for welding applications in building ships and offshore structures.

Fig. 18 shows the z-axis displacement distribution in Case A-1 in the top view and the lines on which strongbacks to be positioned. These lines pass over the area where the largest displacements have been found. Four strongbacks are attached along these lines to strengthen the stiffness in each direction, and the relationship between the positioning strongback and the stiffener size is investigated.

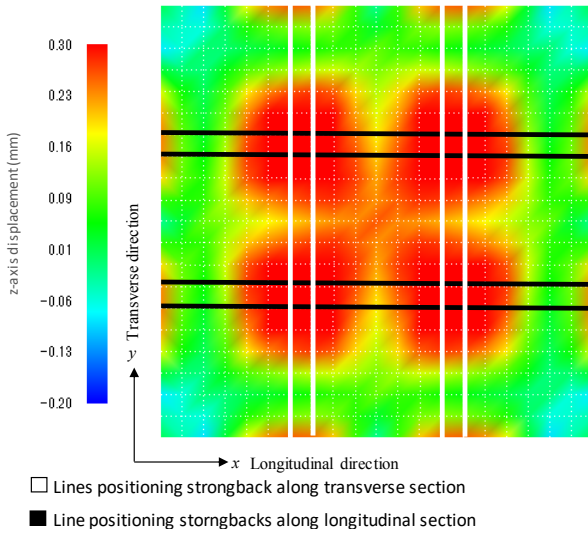


Fig. 18. Lines positioning strongbacks of the square shaped grillage structure

### 5.1 Results and Discussion of the Effect of Strongbacks on the Square-Shaped Grillage Structure

To compare the effect of strongback positioning on the welding displacements of the square-shaped grillage structure,  $A_{displacement}$  is introduced. The z-direction displacement distributions of the bottom plate along the selected two lines, ST and SL shown in Fig. 9, are compared to analyze the effect of strongback positioning for the square-shaped grillage structure precisely.

Three cases B-1, B-2 and B-3 using different length of strongbacks along the longitudinal direction are simulated as shown in Fig. 19. These cases are as follows:

- B-1: Strongback legs are positioned at the maximum points of the displacement curve
- B-2: Strongback legs are positioned outside of the minimum points of the displacement curve
- B-3: Strongback legs are positioned inside of the minimum points of the displacement curve

$A_{displacement}$  of these cases are compared in Fig. 20 where large reduction mitigation is obtained in Case B-3.  $A_{displacement}$  is reduced 37.4% (from 0.147 mm to 0.092 mm) by setting the strongback legs at the positions of  $x = 40 \sim 60$  mm and  $340 \sim 360$  mm. On the other hand, strongbacks of Cases B-1 and B-2 are not so effective since their reductions of  $A_{displacement}$  are only 2.7% and 5.4%, respectively.

The z-axis displacement curves of them are shown in Fig. 19 where the result of analysis without strongback (Case A-1) is also plotted. Case B-1 shows that the presence of the strongbacks has a slight impact on reducing the welding displacements of the center area as can be seen by the two displacement curves with and without strongbacks. In Case B-2, it is observed that there is no impact on the welding displacements in the inner zone (the area between the strongback legs), but there is a decrease in the welding displacement in the outer zone. In Case B-3, it seen that there is a substantial reduction in the welding displacements in the inner zone and a slight increase in the outer zone.

To thoroughly discuss the results of z-axis displacement curves of Cases B-2 and B-3, Fig. 21 is introduced. In Case B-3, the additional strongback leads to the reduction of the angular displacement of 0.0014 rad (38 %) in the inner zone resulting in the descent of the curve. However, this strongback effects on the increase of the angular displacement of 0.0014 rad (64 %) in the outer zone.

In Case B-2, the additional strongback leads to the reduction of the angular displacement of 0.0011 rad (50 %) in the outer zone as similar to Case B-3, but small increase of the angular displacement of 0.000043 rad (1 %) in the inner zone is observed. The reason for the small change of angular displacement in the inner zone is that the inner part connects to the center of the structure which has the high stiffness, and it leads to mitigate the increase of the angular displacement. The large stiffener located just inner side of the leg also disturbs the angular change in the inner zone.

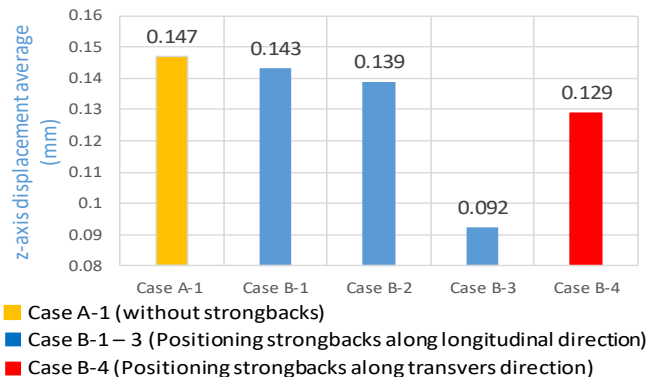


Fig. 20.  $A_{displacement}$  of the square-shaped grillage structure with differently positioned strongbacks

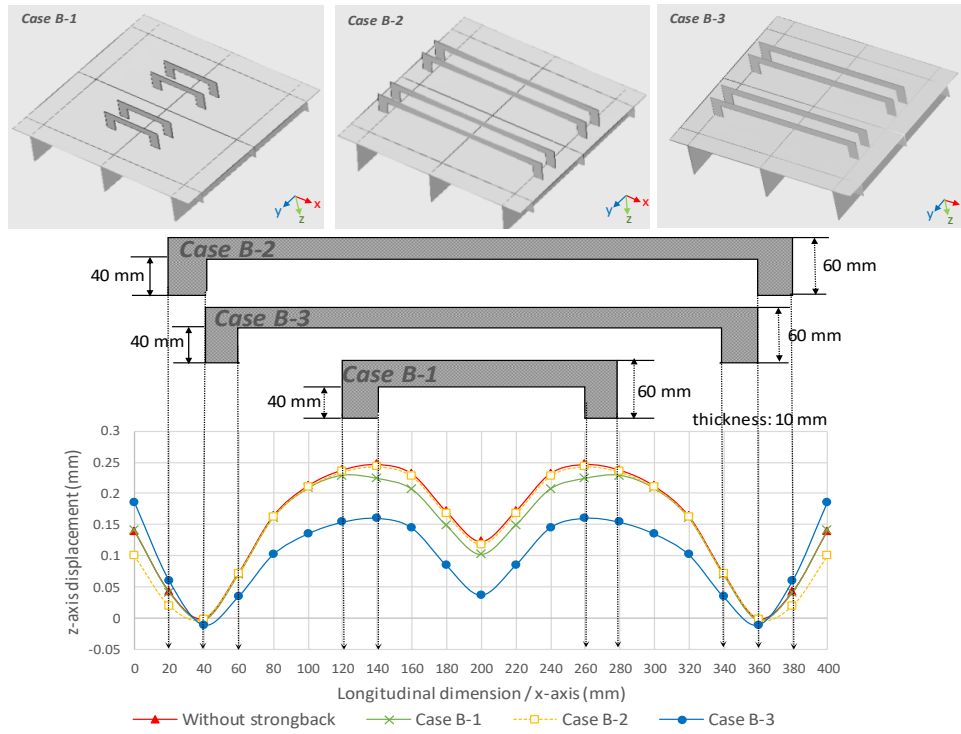


Fig. 19. Positions of strongbacks and z-axis displacement curves of SL in Cases B-1, B-2 and B-3

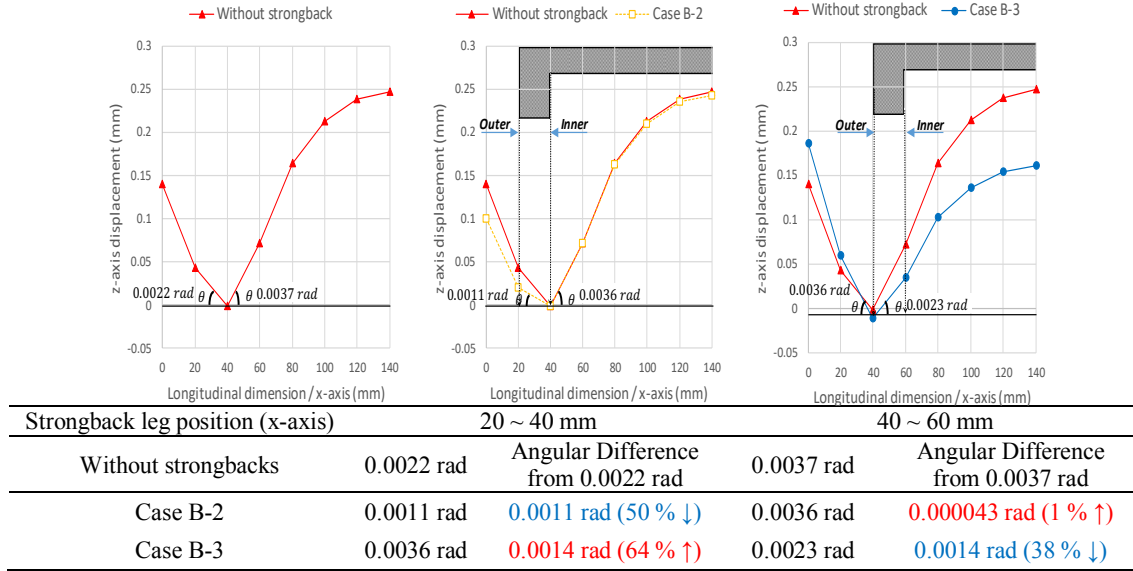


Fig. 21. Effect of strongback on z-axis displacement curves in Case B-2 and B-3

It is expected that strongbacks make the slope of the plate flat at the positions where their legs are attached. Hence, it is tried to use the angular deformation (the slope of the z-axis displacement) without strongbacks for determining the locations of the strongbacks. Fig. 22 shows the angular deformation by welding without strongbacks (Case A-1). The strongback legs of Cases B-1 and B-3 are positioned where the angular deformations are 0.0004 rad and 0.0037 rad, respectively. Three additional three numerical simulations with strongbacks at the positions whose angular deformations of 0.0046 rad, 0.0024 rad and 0.0013 rad are carried out to see the relationship between the angular deformation of Case A-1 and welding displacement. The results of them are shown in Fig. 23 in which the horizontal axis indicates the x coordinates of the positions of the strongback legs. A green dashed line shows the angular deformation without strongback, while a blue solid

line shows the  $A_{displacement}$  in the cases with strongbacks. A negative correlation between the angular deformation and the  $A_{displacement}$  observed. It is clearly seen that the efficiency of the strongback is the highest in the case that its legs are placed at the zone where the largest angular deformation is observed before attaching strongback. In Case B-4, the strongbacks are positioned along the transverse direction as shown in Fig. 24. Their legs are attached at the inside of the minimum points of the displacement curve as similar to Case B-3 that is the most effective in the previous simulations. The tendency of the displacement curve in Case B-4 is somewhat similar to those obtained in Case B-3, with a reduction in welding displacement in the inner zone and a rise in the outer zone; however, the results obtained in Case B-3 are clearly superior to Case B-4. This is due to the fact that the high stiffness of the transverse stiffeners reduces the effect of

placed strongbacks in Case B-4. According to above results and discussions, the systematic method for optimally positioning strongbacks under limited work environment

condition to maximize their efficacy for minimizing welding displacements is proposed as Fig. 25.

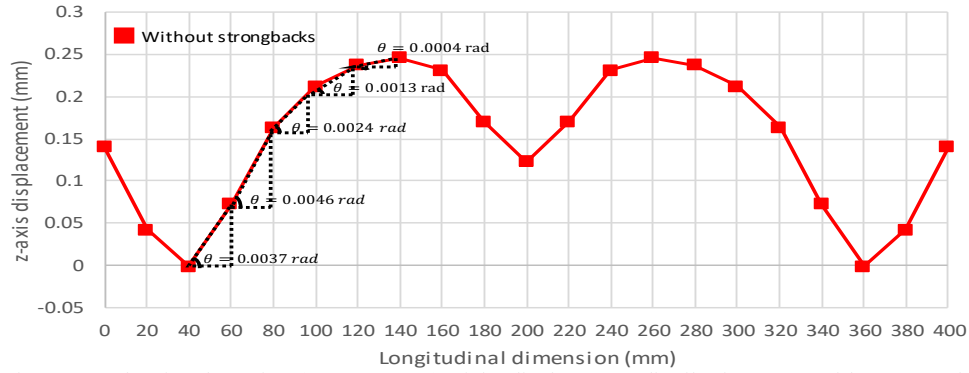


Fig. 22. Angle of each section (40 ~ 140 mm) of the displacement distribution curve without strongbacks

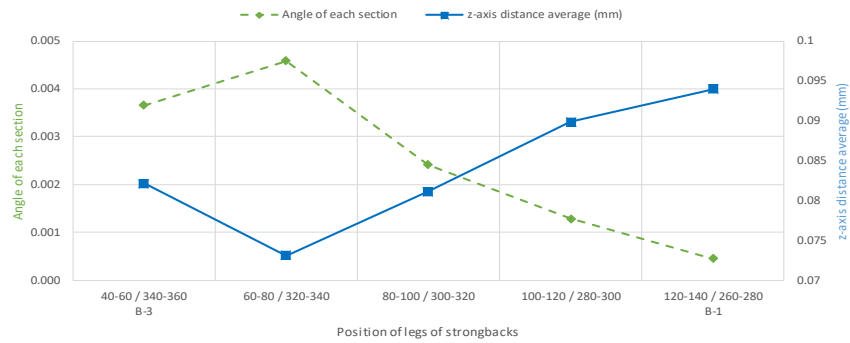


Fig. 23.  $A_{displacement}$  for the square shape grillage structure obtained for each of the five strongbacks positions based on the angle of the displacement curve

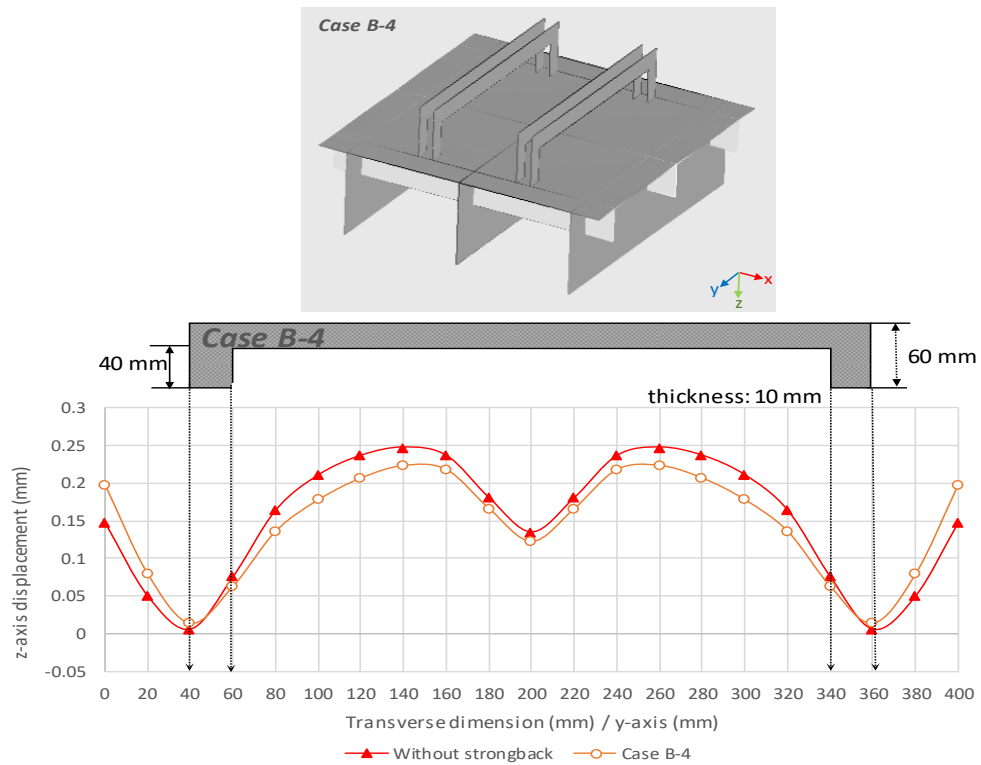


Fig. 24. Position of strongbacks and z-axis displacement curve of ST in Case B-4

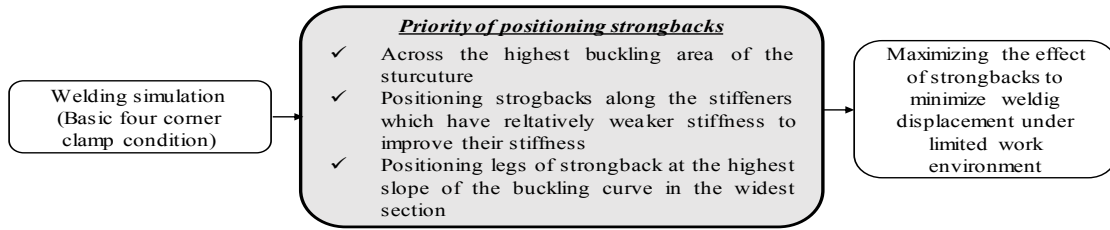


Fig. 25. Systematic method to optimally position strongbacks under limited work environment

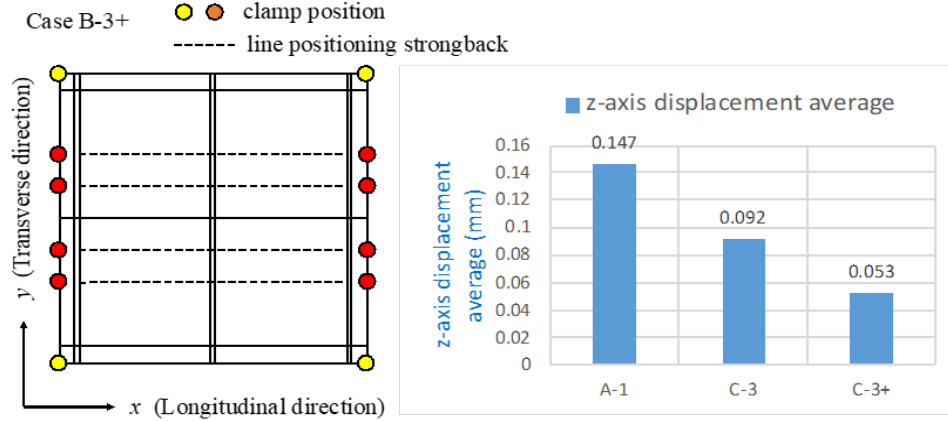


Fig. 26. Combining clamps and strongbacks in Case B-3+ and  $A_{displacement}$

## 6. The Effect of Additional Clamping along Strongbacks on the Square-Shaped Grillage Structure

In Case B-3, the two legs of strongbacks are positioned inside of the location indicated by the minimum points of the displacement curve to provide large mitigation in the welding displacement in the inner zone; however, this led to an increase in the welding displacements in the outer zone. To address this increase in welding displacement in the outer zone, additional clamping is provided as Case B-3+ in Fig. 26.  $A_{displacement}$  is 0.053 mm which is 63.8% reduction from A-1, while  $A_{displacement}$  of Case B-3 is 0.092 mm which is 37.4% reduction from A-1. Hence, an optimal combination of clamps and strongbacks is also effective in reducing the welding displacements.

## 7. Validation of Systematic Method to Efficiently Position Clamps for the reduction of Welding Displacements of the General Ship Grillage Structure under Limited Work Environment

First, the basic clamping condition that clamps four corners of the

bottom plate is applied to the general ship grillage structure. It is noted as Case C-1 and shown in Fig. 27 where yellow circles indicate the basic clamps. Additional clamps are basically positioned at nodes which have the highest displacement along each edge based on the results of these basic clamping conditions. Additional 6 clamps are positioned along longitudinal edges as C-2 in Fig. 28 according to the systematic method proposed in chapter 4 since transverse stiffeners are stronger than longitudinal stiffeners. But, the difference of the moment of inertia of area between the longitudinal and transverse sections is not so large. Case C-3 with additional 8 clamps is used for comparing the effectivity of clamp positioning though the number of additional clamps is more than Case C-2.

C-1: Basic clamps at the corners of bottom plate marked by yellow circles

C-2: Additional 6 clamps along the longitudinal edges marked by blue circles (by the proposed method)

C-3: Additional 8 clamps along the transverse edges marked by red circles

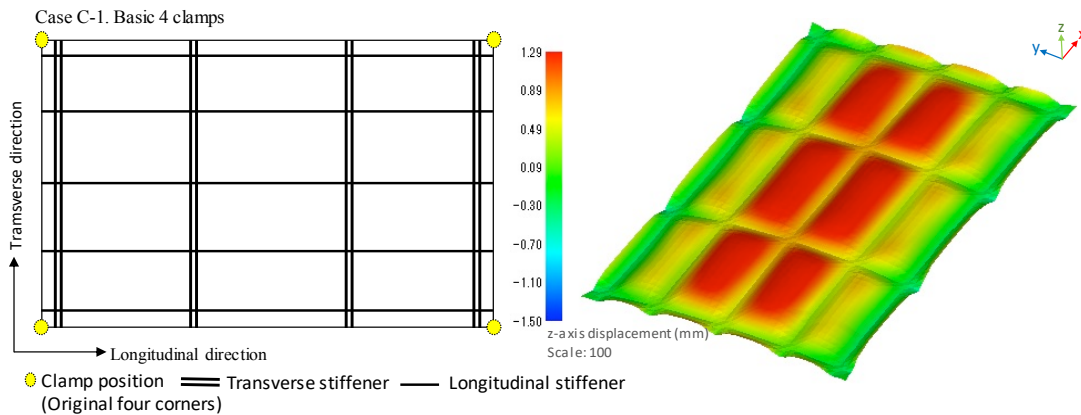


Fig. 27. Z-axis displacement of the bottom plate of Case C-1

## 7.1 Results and Discussion of the Effect of Clamping on the General Ship Grillage Structure

$A_{displacement}$  is used to see the overall effect of the additional clamps on the welding displacements of the general ship grillage structure. Two lines, GT (Transverse) and GL1 (Longitudinal), are selected to analyze the effects of clamp positions as Fig. 29.

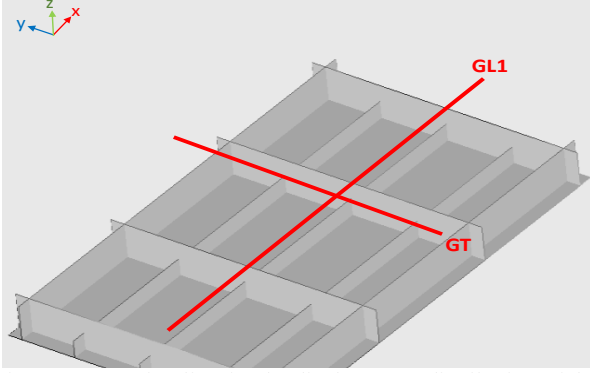


Fig. 29. Measuring line for the displacement distribution of the general ship grillage structure GT and GL1

Fig. 30 shows  $A_{displacement}$  for the three Cases C-1, C-2 and C-3 obtained for the general ship grillage structure. Case C-2 whose clamping positions are determined by the proposed method reduces  $A_{displacement}$  from 0.650 mm to 0.397 mm, while  $A_{displacement}$  of Case C-3 is 0.454 mm. So, the proposed clamping method works well

for the general ship grillage structure, even though Case C-2 has disadvantage in the number of clamps.

In Fig. 31, Case C-2 shows that the additional 6 clamps on the longitudinal edges mitigate buckling feature deformation at both of the longitudinal edges and the center of bottom plate. Case C-3, whose reduction of  $A_{displacement}$  is 30.2%, shows that the additional 8 clamps on the transverse edges successfully mitigate local z-axis displacement of transverse edges but the reduction of the center buckled feature deformation is less than Case C-2. Focusing on the edges of plate, Case C-2 suppresses the z-axis displacement, but Case C-3 generates a large displacement in the negative direction along longitudinal edges.

Fig. 32 and 33 show the z-axis displacement distributions of Cases C-1, C-2 and C-3 along the lines of GT and GL1, respectively. Case C-2 based on the proposed method shows the good performance along both lines except for the end points of GL1 where the additional clamps are given in Case C-3.

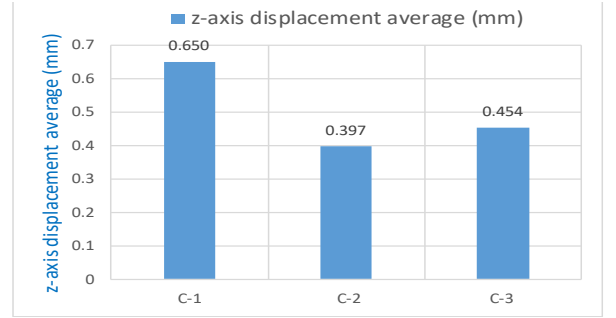


Fig. 30.  $\bar{A}_{displacement}$  of the general ship grillage structures

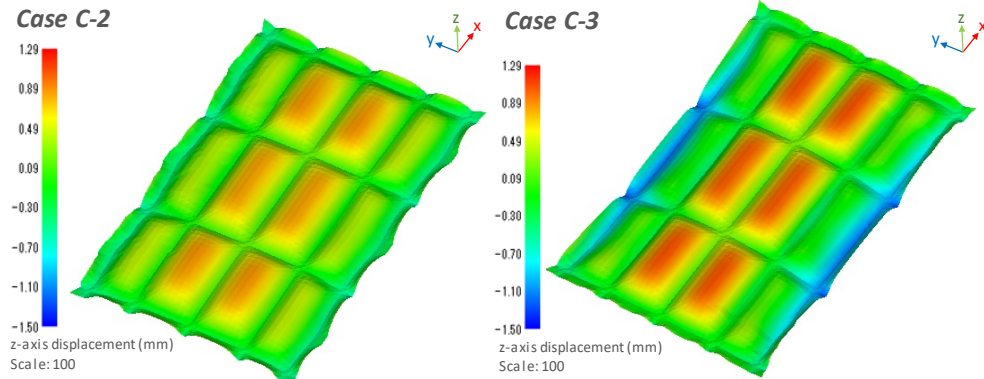


Fig. 31. Z-axis displacement of the bottom plate of Case C-2 and C-3

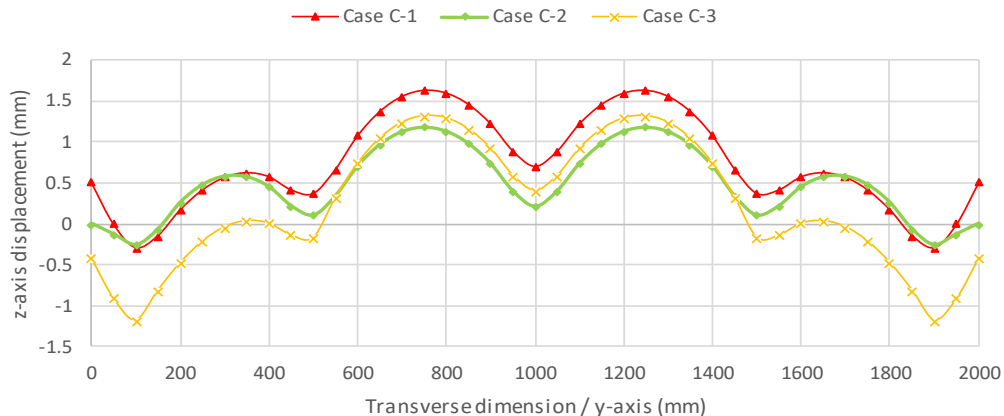


Fig. 32. Z-axis displacement distribution of GT



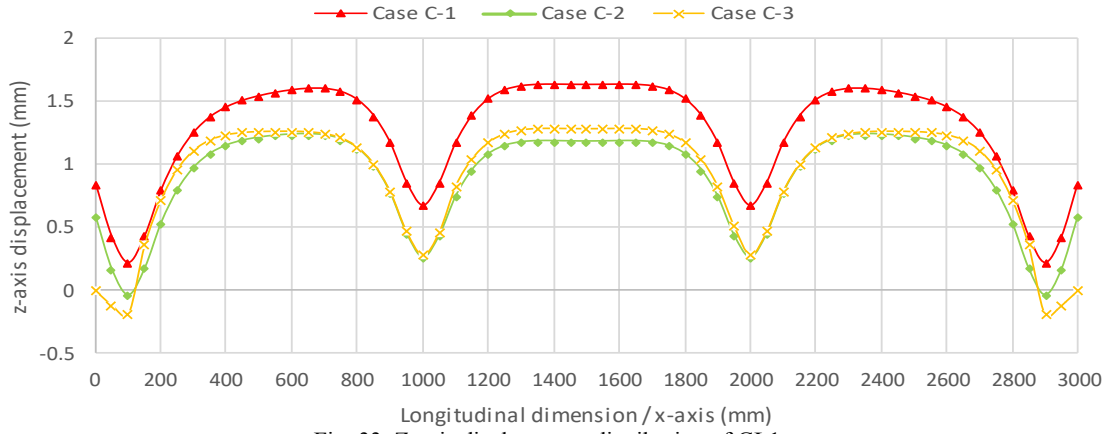


Fig. 33. Z-axis displacement distribution of GL1

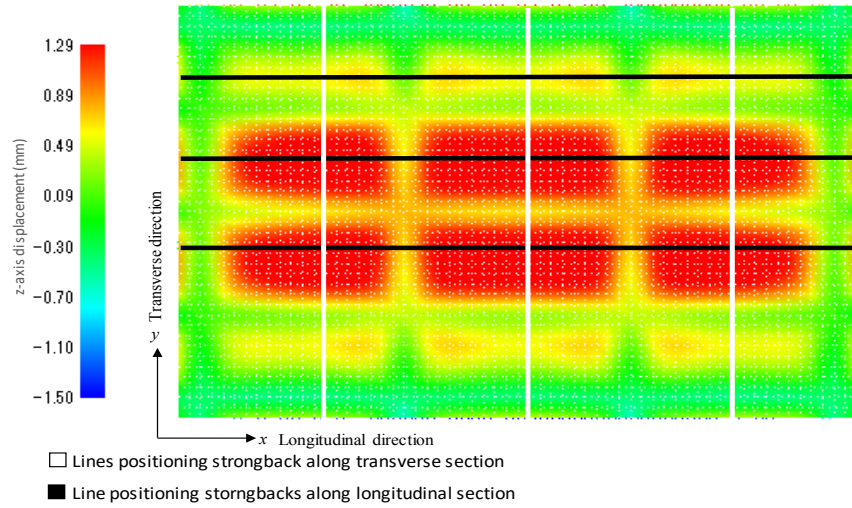


Fig. 34. Lines positioning strongbacks of the general ship grillage structure

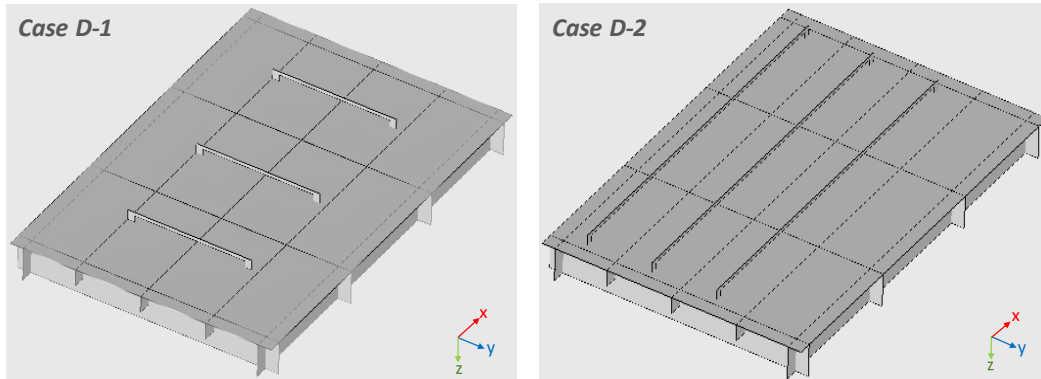


Fig. 35. Strongbacks positioning in Cases D-1 and D-2

## 8. Validation of Systematic Method to Efficiently Position Strongbacks for the reduction of Welding Displacements of the General Ship Grillage Structure under Limited Work Environment

Fig. 34 shows the distribution of z-direction displacement of Case C-1 in the top view. Three strongbacks along the transverse direction and the longitudinal direction are positioned, respectively, as shown in Fig. 35 such that they across the highest displacement zones of each section of the general ship grillage structure to minimize the global welding displacements. The efficiency of the directions of the strongbacks is evaluated.

D-1: Strongback legs are positioned at the maximum slope of the displacement curve along the transverse direction

D-2: Strongback legs are positioned at the maximum slope of the displacement curve along the longitudinal direction (by the proposed method)

Case D-2 has the strongback position according to the method proposed in chapter 7 since the longitudinal stiffeners are weaker than transverse stiffeners. Since three strongbacks are used for both cases to give the same condition to two cases, the layout of strongbacks in Case D-2 may not be the best.



## 8.1 Results and Discussion of the Effect of Strongbacks on the General Ship Grillage Structure

$A_{displacement}$  is used to see the overall effect of the additional strongbacks on the welding displacements. The z-direction displacement distributions of the bottom plate along the selected two lines, GT (Transverse) and GL2 (Longitudinal) shown in Fig. 36, are used to analyze the effects of strongback positions.

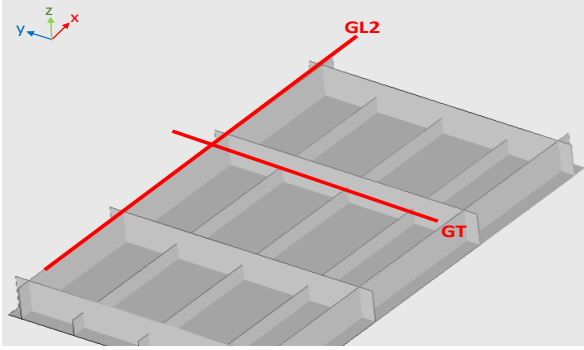


Fig. 36. Measuring line for the displacement distribution of the general ship grillage structure GT and GL2

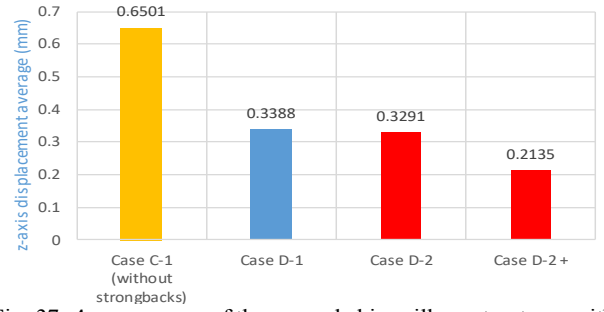


Fig. 37.  $A_{displacement}$  of the general ship grillage structures with differently positioned strongbacks

$A_{displacement}$  of Cases D-1 and D-2 are 0.339 mm and 0.329 mm, respectively, as shown in Fig. 37. So, Case D-2 based on the proposed method shows better performance than Case D-1 just a little bit. Fig. 38 and 39 show the positions of strongbacks and the z-axis displacements along GT and GL2, respectively. It is clearly shown that the strongbacks in both cases are very effective to mitigate the welding deformations along both lines in the inner zones of their legs. Case D-2 has the disadvantage such that the number of strongbacks and the number of sections between stiffeners don't match, while one strongback is set for each high displacement area in Case D-1. Despite this unfavorable condition,  $A_{displacement}$  of Case D-2 is smaller than D-1. So, the effectivity of the proposed method for reducing welding deformation by strongbacks is seen in the general ship grillage structure.

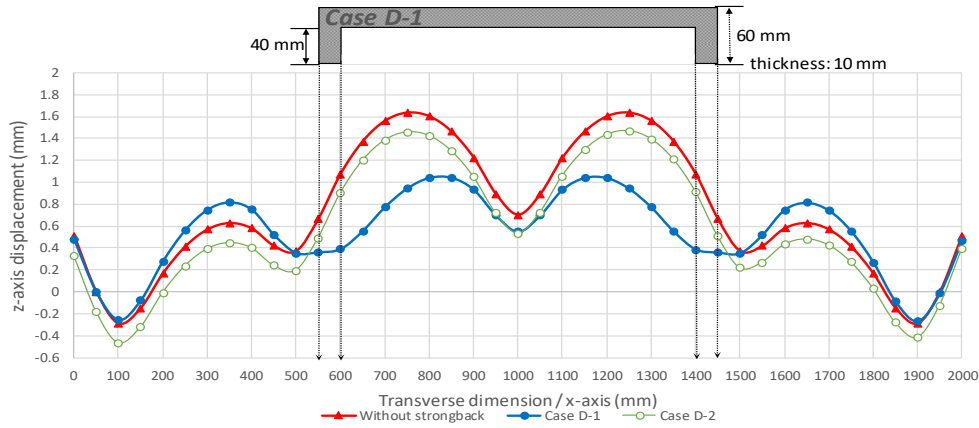


Fig. 38. Positions of strongbacks and z-axis displacement curve of Cases D-1 and D-2 along GT

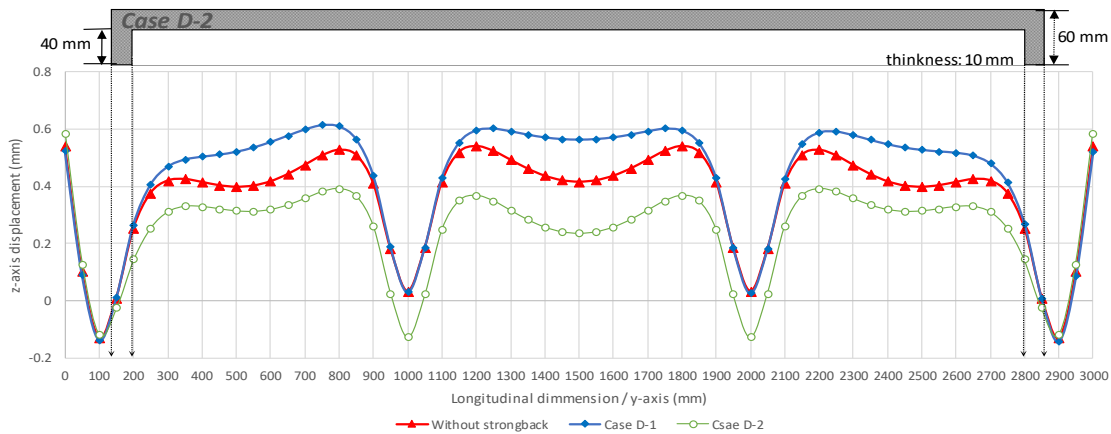


Fig. 39. Positions of strongbacks and z-axis displacement curve of Cases D-1 and D-2 along GL2

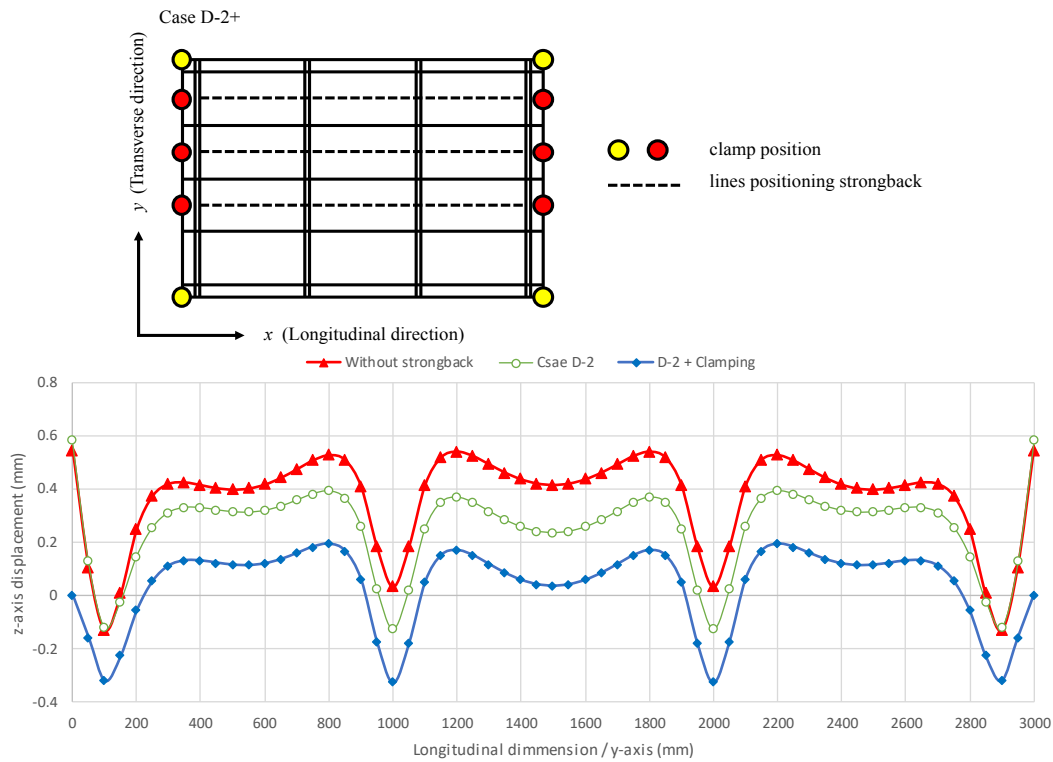


Fig. 40. Combining clamps and strongback and z-axis displacement curves of Case D-2+ along GL2

## 9. Validation of the effect of additional clamping along strongbacks on the General Ship Grillage Structure

To validate the efficacy of the combination of clamps with strongbacks in the general ship grillage structure. Case D-2+ is created by adding clamps along the edges near the ends of strongbacks in Case D-2. Fig. 40 shows that the z-axis displacement distribution curve of Case D-2+ close the zero line, and the overall welding displacement has been greatly reduced.  $A_{displacement}$  is 0.2135 mm, which is 64.9% of Case D-2. Hence, an optimal combination of clamps and strongbacks is very effective in reducing the welding displacements.

## 10. Conclusion

In the present study, the systematic method to optimally position clamps and strongbacks that results in minimal welding displacements was proposed. Several cases were numerically simulated using the theory of inherent strain, interface-element method, and MPC to study the effect of clamps and strongbacks and help identify the optimal placements for these external constraints. This study contributes to the understanding of the role of clamps and strongbacks in welding displacement reduction. The conclusions are:

1. Positioning additional clamps obviously reduce  $A_{displacement}$ . In particular, the efficiency of additionally positioned clamps highly depends on the relationship between the size of stiffeners (placed in both of the longitudinal and transverse directions) and the position of additional clamps.
2. Based on positioning clamps at the highest displacement points along edges of the welded structure, clamps along edges perpendicular to the stiffeners which have relatively larger stiffness efficiently improve their role to mitigate welding displacement.

3. Strongbacks lead to the reduction of  $A_{displacement}$  by influencing the displacement distribution curve.
4. Positioning legs of strongbacks at the largest slope section of the displacement distribution curve maximizes the efficiency of strongbacks for minimizing welding displacements.
5. The extension of the area influenced by the strongback to mitigate the z-axis displacement curve is limited by the stiffeners. Thus, positioning strongbacks at the widest section which isn't separated by stiffeners improves their efficacy.
6. The efficiency of strongbacks becomes relatively weaker when they are placed along the stiffest section of the structure as the transverse section herein.
7. Combining optimally positioned clamps and strongbacks along the same line is effective in minimizing welding displacements.

## References

- Chen, Zhen, Chen, Zhechao, Sheno, R.A., 2015. Influence of welding sequence on welding deformation and residual stress of a stiffened plate structure. *Ocean Eng.* <https://doi.org/10.1016/j.oceaneng.2015.07.013>
- Deng, D., Murakawa, H., Liang, W., 2007. Numerical simulation of welding distortion in large structures. *Comput. Methods Appl. Mech. Eng.* <https://doi.org/10.1016/j.cma.2007.05.023>
- Deng, D., Murakawa, H., Ueda, Y., 2004. Theoretical prediction of welding distortion considering positioning and gap between parts. *Int. J. Offshore Polar Eng.*
- Hajduk, M., Semjon, J., Vagaš, M., 2011. Design of the welding fixture for the robotic stations for spot welding based on the modular concept. *Acta Mech. Slovaca.* <https://doi.org/10.2478/v10147-010-0044-y>
- Kunihiko, Satoh, Terasaki, T., 1976. Effect of welding conditions on residual stresses distributions in welded structures materials. *J. JAPAN Weld. Soc.* <https://doi.org/10.2207/qjwjs1943.45.150>

- Liang, W., Deng, D., Sone, S., Murakawa, H., 2005. Prediction of welding distortion by elastic finite element analysis using inherent deformation estimated through inverse analysis. *Weld. World*. <https://doi.org/10.1007/BF03266500>
- Liu, C., Zhang, J.X., 2009. Numerical simulation of transient welding angular distortion with external restraints. *Sci. Technol. Weld. Join*. <https://doi.org/10.1179/136217108X341175>
- Luo, Y., Murakawa, H., Ueda, Y., 1997. Prediction of welding deformation and residual stress by elastic FEM based on inherent strain (Report I). *Trans. JWRI*.
- Ma, N., Huang, H., 2017. Efficient simulation of welding distortion in large structures and its reduction by jig constraints. *J. Mater. Eng. Perform*. <https://doi.org/10.1007/s11665-017-3000-4>
- Ma, N., Huang, H., Murakawa, H., 2015. Effect of jig constraint position and pitch on welding deformation. *J. Mater. Process. Technol*. <https://doi.org/10.1016/j.jmatprotec.2015.02.022>
- Michaleris, P., 2011. Minimization of welding distortion and buckling: modelling and implementation, minimization of welding distortion and buckling: Modelling and implementation. <https://doi.org/10.1533/9780857092908>
- Murakawa, H., Deng, D., Ma, N., Wang, J., 2012. Applications of inherent strain and interface element to simulation of welding deformation in thin plate structures. *Comput. Mater. Sci*. <https://doi.org/10.1016/j.commatsci.2011.06.040>
- Park, J.U., An, G., Lee, H.W., 2012. Effect of external load on angular distortion in fillet welding. *Mater. Des*. <https://doi.org/10.1016/j.matdes.2012.06.006>
- Schenk, T., Richardson, I.M., Kraska, M., Ohnimus, S., 2009. A study on the influence of clamping on welding distortion. *Comput. Mater. Sci*. <https://doi.org/10.1016/j.commatsci.2009.01.004>
- Ueda, Y., Yuan, M.G., Mochizuki, M., Umezawa, S., Enomoto, K., 1993. Experimental verification of a method for prediction of welding residual stresses in T joints using inherent strains 4th report: Method for prediction using source of residual stress. *Weld. Int*. <https://doi.org/10.1080/09507119309548506>
- Wang, J., Rashed, S., Murakawa, H., 2011. Investigation of buckling deformation of thin plate welded structures. *Proceeding 21st Int. Soc. Ocean Polar Eng*.
- White, J.D., Leggatt, R.H., Dwight, J.B., 1980. Weld shrinkage prediction. *Weld. Met. Fabr*.
- Woo, D.H., Kitamura, M., Takezawa, A., 2019. Method to systemically order welding sequence to mitigate welding displacement of a general ship grillage structure. *Ships and offshore structures*. <https://doi.org/10.1080/17445302.2019.1681865>.
- Ye, Y., Cai, J., Jiang, X., Dai, D., Deng, D., 2015. Influence of groove type on welding-induced residual stress, deformation and width of sensitization region in a SUS304 steel butt welded joint. *Adv. Eng. Softw*. <https://doi.org/10.1016/j.advengsoft.2015.04.001>
- Japan Shipbuilding Research Association 237 Research Subcommittee (SR 237): Research on advanced manufacturing accuracy management technology (Total Annual Report), Japan Shipbuilding Research Association, 2000